tvst

DOI: 10.1167/tvst.4.5.2

Article

Restricted Summed-Area Projection for Geographic Atrophy Visualization in SD-OCT Images

Qiang Chen[1], Sijie Niu[1], Honglie Shen[1], Theodore Leng[3], Luis de Sisternes[2], and Daniel L. Rubin[2]

[1] School of Computer Science and Engineering, Nanjing University of Science and Technology, Nanjing, China
[2] Department of Radiology and Medicine (Biomedical Informatics Research), Stanford University School of Medicine, Stanford, CA, USA
[3] Byers Eye Institute at Stanford, Stanford University School of Medicine, Palo Alto, CA, USA

Correspondence: Qiang Chen, School of Computer Science and Engineering, Nanjing University of Science and Technology, 200 Xiao Ling Wei, Nanjing 210094, China; chen2qiang@njust.edu.cn

Received: 14 January 2015
Accepted: 21 June 2015
Published: 1 September 2015

Keywords: geographic atrophy visualization; spectral domain optical coherence tomography; restricted summed-area projection; choroidal vasculature; geographic separability

Citation: Chen Q, Niu S, Shen H, Leng T, de Sisternes L, and Rubin DL. Restricted summed-area projection for geographic atrophy visualization in SD-OCT images. 2015;4(5):2, doi:10.1167/tvst.4.5.2

Purpose: To enhance the rapid assessment of geographic atrophy (GA) across the macula in a single projection image generated from three-dimensional (3D) spectral-domain optical coherence tomography (SD-OCT) scans by introducing a novel restricted summed-area projection (RSAP) technique.

Methods: We describe a novel en face GA visualization technique, the RSAP, by restricting the axial projection of SD-OCT images to the regions beneath the Bruch's membrane (BM) boundary and also considering the choroidal vasculature's influence on GA visualization. The technique analyzes the intensity distribution beneath the retinal pigment epithelium (RPE) layer to fit a cross-sectional surface in the sub-RPE region. The area is taken as the primary GA projection. A median filter is then adopted to smooth the generated GA projection image. The RSAP technique was evaluated in 99 3D SD-OCT data sets from 27 eyes of 21 patients presenting with advanced nonexudative age-related macular degeneration and GA. We used the mean difference between GA and background regions and GA separability metric to measure GA contrast and distinction in the generated images, respectively. We compared our results with two existing GA projection techniques, the summed-voxel projection (SVP) and Sub-RPE Slab techniques.

Results: Comparative results demonstrate that the RSAP technique is more effective in displaying GA than the SVP and Sub-RPE Slab. The average of the mean difference between GA and background regions and the GA separability based on SVP, Sub-RPE Slab, and RSAP were 0.129/0.880, 0.238/0.919, and 0.276/0.938, respectively.

Conclusions: The RSAP technique was more effective for GA visualization than the conventional SVP and Sub-RPE Slab techniques. Our technique decreases choroidal vasculature influence on GA projection images by analyzing the intensity distribution characteristics in sub-RPE regions. The generated GA projection image with the RSAP technique has improved contrast and distinction.

Translational Relevance: Our method for automated generation of GA projection images from SD-OCT images may improve the visualization of the macular abnormalities and the management of GA.

Introduction

Age-related macular degeneration (AMD) is the leading cause of blindness among the elderly. Advanced AMD, where vision loss is mostly noticed, is most common in a nonexudative form characterized by the presence of geographic atrophy (GA).[1–3] Here, atrophy refers to the degeneration of the deepest cells of the retina. To date, the primary retinal layer affected by the evolution of GA remains unclear; GA represents the loss of either photoreceptors (PR), retinal pigment epithelium (RPE), or choriocapillaris layers within the macula.[4–6] However, most histopathological studies suggest that the initial event in GA occurrence is RPE cell loss, followed with ensuing PR cell death and choriocapillaris atrophy.[7–9]

In the recent years, spectral-domain optical coher-

ence tomography (SD-OCT) has become the preferable imaging method to acquire high-speed, high-resolution, high-density three-dimensional (3D) images covering the central macula[10] and has proven successful in identifying the GA.[11] Bearelly et al.[6] studied the PR-RPE interface in GA using SD-OCT to test in vivo to determine if SD-OCT provides an adequate resolution for reproducible measurement of the PR layer at the margins of GA. Fleckenstein et al.[12,13] used SD-OCT to describe a wide spectrum of morphologic alterations that appear within the atrophic area, as well as within the surrounding retinal tissue. Traditionally, progression and enlargement of GA has been assessed on fundus autofluorescence images (FAF).[14] FAF has remained the gold standard for direct GA visualization, as it demarcates the lesion borders more precisely than clinical observation on fundus photography taking advantage of the optical properties of lipofuscin and photoreceptor degeneration products.[15] Schmitz-Valckenberg et al.[16] compared the FAF and OCT appearance of eyes with GA, and showed that the mean length of an atrophic lesion measured on the FAF image had the closest agreement with the appearance of choroidal hyperreflectivity on the OCT B-scan, and the reduction of the FAF signal seen from GA was spatially correlated with the abrupt transition on the SD-OCT B-scan from a hyporeflective choroid to a hyperreflective choroid. Sayegh et al.[17] concluded that SD-OCT seems to be an appropriate imaging modality for evaluating the extent of GA lesions, and the area of choroidal signal enhancement on the SD-OCT B-scans correlated well with the hypofluorescence area measured on FAF. Color fundus photographs (CFPs) can also be used for GA visualization and assessment; however, it is difficult to make reproducible quantitative measurements of GA in CFPs.[18]

SD-OCT imaging can produce a fundus image (OFI) for visualizing GA by generating an en face summed-voxel projection (SVP) of all the B-scans.[6,19–21] However, the SVP fundus images may not ideal for GA assessment as other retinal pathologies with high reflectivity, such as drusen, may interfere with GA visualization. Stopa et al.[22] overcame this problem by identifying pathologic retinal features with color markings in each B-scan image before the image volume was collapsed along the depth axis to produce the SVP. While effective, this technique is time consuming because of the human interaction required. A newer technique introduced into OCT imaging devices is the Sub-RPE Slab, which creates an en face image only from the light reflected from beneath the RPE. The Sub-RPE Slab has higher contrast at the borders of GA than the conventional SVP technique by excluding the highly reflective retinal layers above the RPE.[23] To increase the contrast further, the Sub-RPE Slab technique was improved by combining choroidal brightening and RPE thinning.[24] However, RPE thinning is not always seen in all areas of GA, so it can only be used as an auxiliary characteristic for GA visualization. Stetson et al.[25] recently presented an OCT minimum intensity (MI) projection to predict locations of growth at the margin of GA and the growth rate outside the margin. The MI image is suitable for observing the margin for GA growth, but is limited by low contrast between GA regions and background regions.

Although the Sub-RPE Slab technique can generate an en face GA projection image with better contrast than the Stetson technique and the SVP fundus image, it does not consider choroidal vasculature, which has low reflectivity and results in decreased contrast within GA regions. In this paper, we present a new fundus projection method, called restricted summed-area projection (RSAP), which improves GA visualization by considering the contribution of the choroidal vasculature to a GA projection image.

Materials and Methods

Anatomically, the choroid can be divided into two principal components: the choriocapillaris, a lobular, vascular plexus comprised of large fenestrated capillaries adjacent to Bruch's membrane (BM), and the choroidal stroma.[26] The main principle of the existing fundus projection GA visualization techniques generated from SD-OCT images lies in the identification of the typical choroidal brightening that appears in the regions affected by GA. However, the many blood vessels in the choroid, which normally manifest in low reflection values, decrease the contrast and distinction of macular regions affected by GA. As an example, Figure 1 shows the choroidal vasculature influence on GA visualization, where Figures 1A and 1B are the SVP and Sub-RPE Slab projection images generated from one 3D SD-OCT scan acquired with a Cirrus OCT (Carl Zeiss Meditec, Inc., Dublin, CA) system, respectively. The RPE boundaries were delineated by hand. Figure 1C displays the B-scan corresponding to the yellow dashed line in Figure 1A, and several structures that can be observed in this image are manually labeled and shown in Figure 1D. We can observe that the contrast (difference between bright

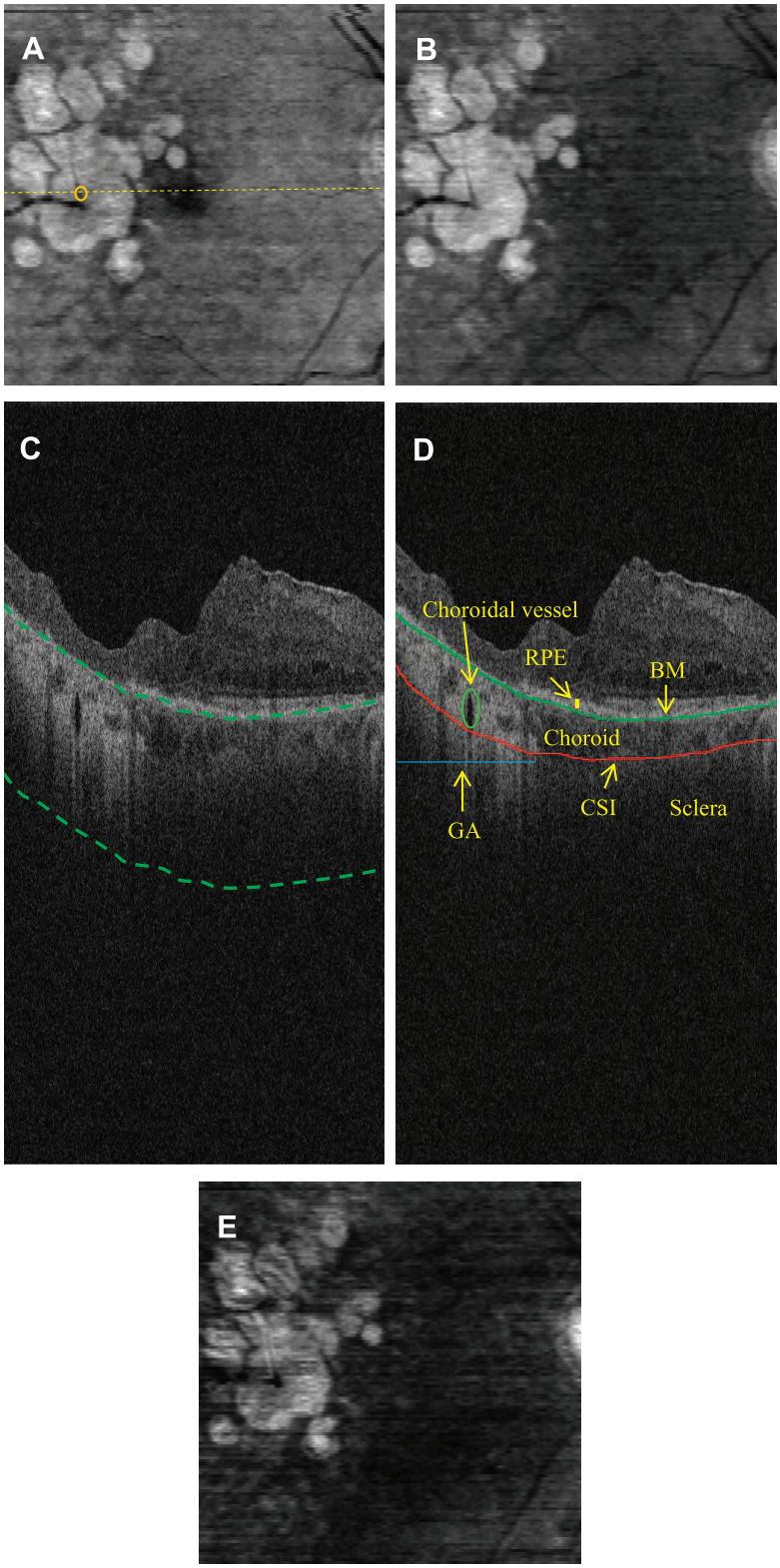

Figure 1. Choroidal vasculature influence on GA visualization. (A) SVP projection image. (B) Sub-RPE Slab projection image. (C) Example B-scan. (D) Example B-scan with structure labels. (E) Sub-CSI Slab projection image.

regions where GA is present and darker background regions) of the Sub-RPE Slab projection image is better than that of the SVP projection image, because the Sub-RPE Slab projection excludes the highly reflective layers above RPE, such as the retinal nerve fiber layer (RNFL) and ellipsoid zone (EZ), which may influence visualization as they are added onto the projection image. Due to the presence of the choroidal vasculature within the region affected by GA, we can observe dark regions within the GA extent in both of the projection images, as marked with the orange circle in Figure 1A.

In order to overcome the influence of the choroidal vasculature on GA visualization, one could follow two different strategies: (1) excluding the choroidal vasculature with a new Sub- Choroidal-Sclera Interface (CSI) Slab technique, similar to that done with the Sub-RPE Slab technique, but restricting the projection region beneath the CSI boundary, or (2) detecting and filling the dark regions where choroidal vessels are present with high intensity values. With the first strategy, the choroidal vasculature would be completely excluded because no vessels appear beneath the CSI boundary, but the main characteristic of GA in SD-OCT imaging, choroidal brightening, would also be omitted. As less light penetrates through the choroid, the brightening difference between the regions inside and outside GA would also be less dramatic, reducing contrast. An example illustrating this effect is shown in Figure 1E, where the image produced by the Sub-CSI Slab projection technique shows less contrast for GA visualization than the earlier proposed techniques (Figs. 1A, 1B). The CSI boundaries for Sub-CSI Slab projection were delineated manually. The Sub-RPE (Fig. 1B) and Sub-CSI (Fig. 1E) projections are to generate the en face image by collapsing the pixels beneath the RPE and CSI, respectively. It does not mean pixel intensity is only plotted along the identified boundaries (RPE or CSI). The pixels in the narrow band beneath the RPE or CSI are collapsed to generate the projection images. In this work we focus on the second proposed strategy, forming an image based in the projection of intensity values restricted to the choroid region, while also detecting and filling with high intensity values the darker regions within the extent of GA that are caused by vessel presence. We call this technique the restricted summed-area projection (RSAP).

GA Visualization Based on RSAP

The main strategy of the RSAP technique lies in using the intensity distribution beneath the RPE layer as observed in SD-OCT images to fill the low intensity regions produced by the presence of choroidal vessels. Vessel presence is identified by analyzing intensity profiles. An example of intensity distribution beneath the RPE in a typical SD-OCT scan, namely the region between the two dashed green curves in Figure 1C, where GA is present is displayed in Figure 2. We can observe that the intensity distribution decreases toward the x direction (depth), and the rate of this decrease in the GA region is typically slower than that in the normal region. Figures 3A and 3B show two intensity profiles (marked with the red curve) of the sub-RPE region (Fig. 2A) in the GA and the normal regions, respectively. The large concave region pointed out in Figure 3A corresponds to the choroidal vessel marked with the orange oval in Figure 1D. This vessel would have a great influence on GA visualization that is solely based on intensity summation, such as with the SVP and Sub-RPE Slab methods. It can be seen from Figure 3 that for the same x position in the choroidal region (axial location) the intensity values in the GA region (Fig. 3A) are larger than those in the normal region (Fig. 3B), except in particular axial locations (x axis) where choroidal vessel regions are located (marked with the orange oval circle in Fig. 1D and the dashed black circle in Fig. 3A). In other words, regions where GA is present will have higher intensity profiles than those where GA is not present, while vessel location can be identified with the presence of local minimums in such profiles. This principle constitutes the basic idea of the proposed RSAP technique.

The flowchart of our technique is shown in Figure 4, which comprises the following operations:

(1) Segmentation of BM boundary: the BM boundaries were segmented with the automatic 3D graph search method[27];
(2) Flattening of sub-RPE region: an image is composed by taking the recorded intensity values beneath the segmented BM boundary up to a maximum depth where GA can be detected, constituting a flattened sub-RPE image. This maximum depth is set up as an independent parameter in this work (depth of sub-RPE, as explained in the later parameter evaluation). The flattened sub-RPE region is shown in Figure 2A;
(3) Finding local maximum intensity points. For each column in the flattened sub-RPE region (A-scan location), the points with local maximum intensity value (namely the intensity value of the point is larger than those of its two connected points)

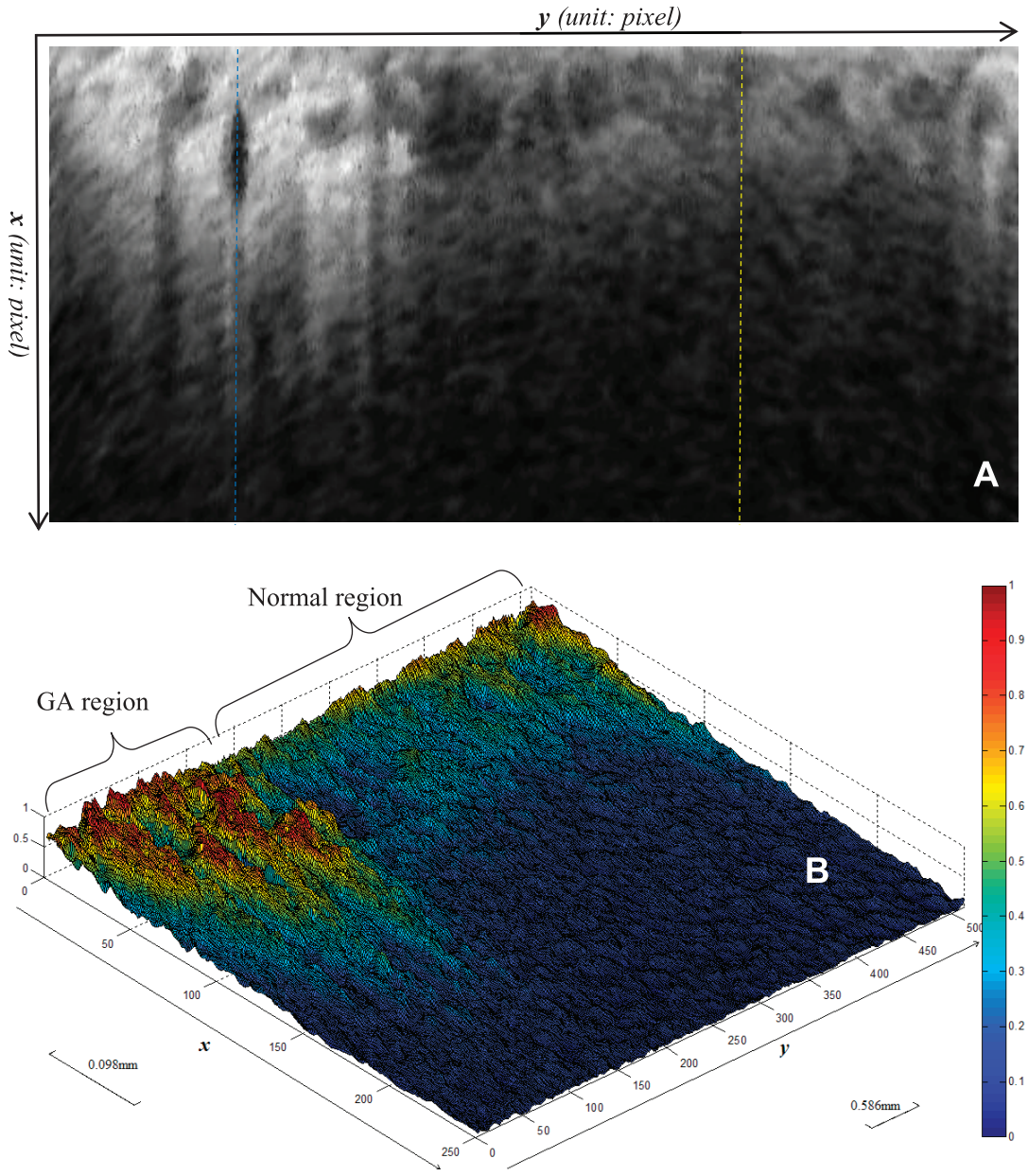

Figure 2. Intensity distribution analysis. (A) Flattened sub-RPE region. (B) Intensity surface of (A).

are found, as marked with the blue circle in Figure 3;

(4) Locating maximum intensity points at higher depths. The maximum intensity points whose value follows a constantly decreasing function with depth (x axis) are selected, as marked with the magenta stars in Figure 3. The purpose of this step is to ensure a constantly descendent intensity profile beneath RPE;

(5) Calculating the area below the surface constructed with the maximum intensity points at higher depths. We interpolate the intensity profile in the axial locations between the selected maximum intensity points at higher depths using linear interpolation (magenta lines in Fig. 3), and calculate the area of the polygon formed by this interpolation and a baseline of zero intensity (area below the magenta lines marked in Fig. 3);

(6) Taking the calculated area above as the primary GA projection value at each projection location; and

(7) Using a median filter to smooth the generated GA projection image: to alleviate the noise influence and make the final GA projection image smoother,

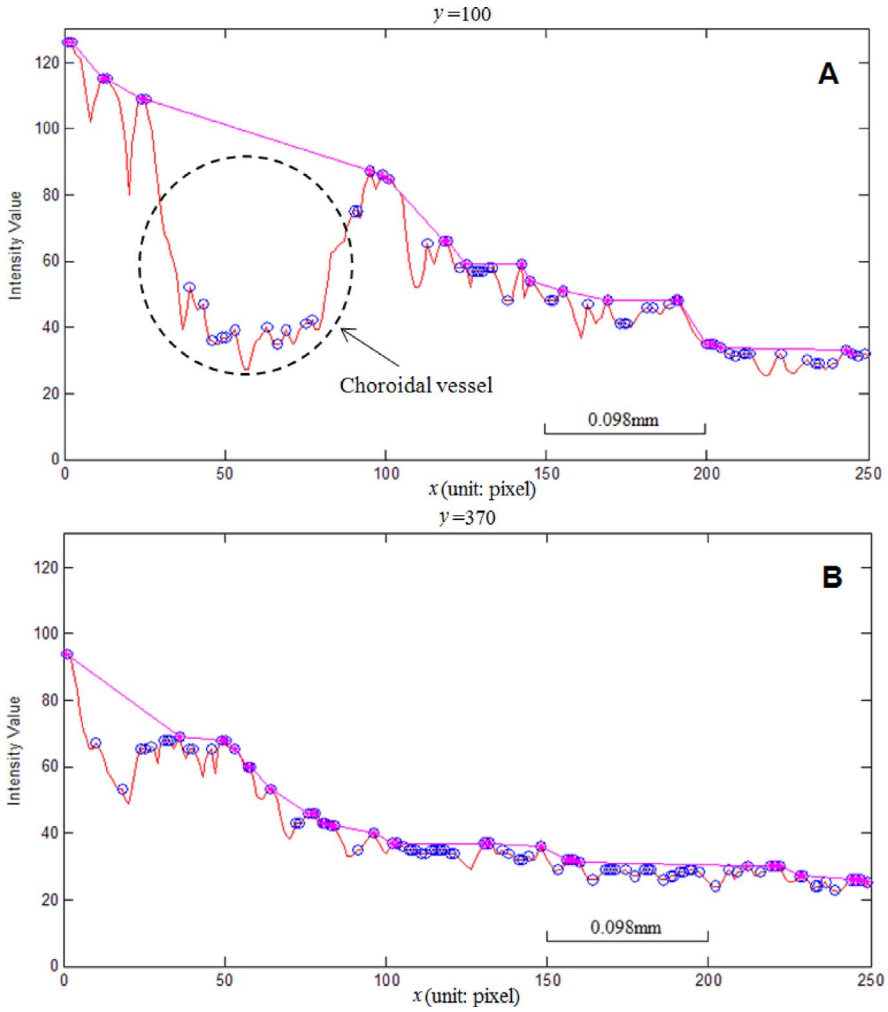

Figure 3. Intensity profiles of columns #100 (A) and #370 (B), marked with the *dashed blue* and *yellow lines* in Figure 2A, respectively. *Red curve*: intensity values of two columns. *Blue circle*: local maximum intensity point. *Magenta star*: maximum intensity point at higher depths (in the x direction). (A) Intensity distribution in GA region. (B) Intensity distribution in normal region.

a simple median filter with a 3×3 neighborhood was used.

Figure 5A shows the GA projection image with the proposed RSAP technique, and Figure 5B shows a detail comparison of three GA projection techniques in regions of interest corresponding to the red dashed rectangles in Figure 6A. Compared with the SVP and Sub-RPE Slab projection images (Figs. 1A, 1B), the RSAP projection image displays a higher contrast and also overcomes the influence of the choroidal vasculature on GA visualization, as shown in Figure 5B.

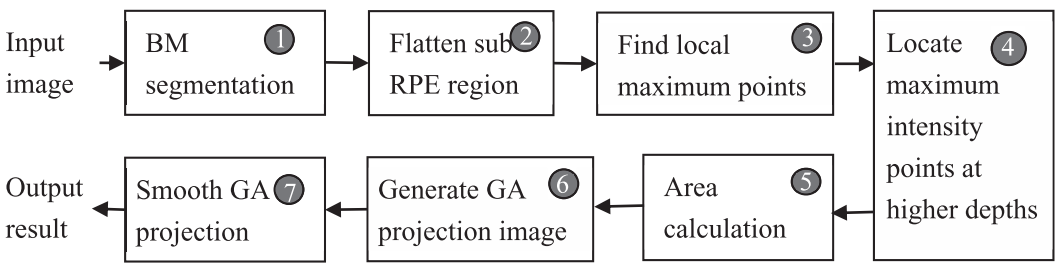

Figure 4. Flowchart of the proposed technique.

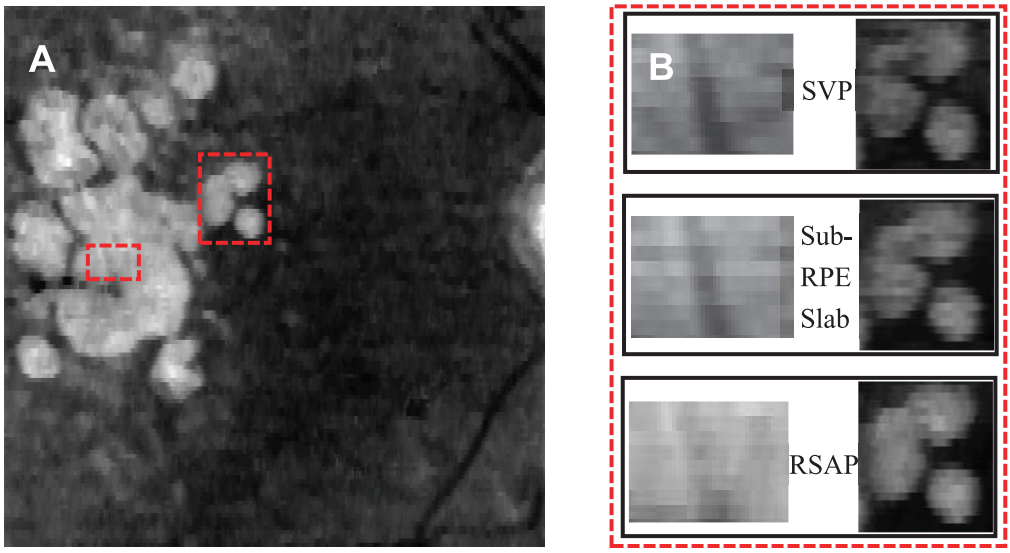

Figure 5. GA projection image with RSAP. (A) RSAP projection image. (B) Results by the three discussed techniques in regions of interest as indicated in (A).

Evaluation Study

To evaluate the RSAP technique for GA visualization, 99 3D SD-OCT macular images from 27 eyes of 21 patients presenting with advanced nonexudative AMD were collected and analyzed. The data was acquired longitudinally, with several observations from the same eye, as a GA was followed up in regular clinical practice. All eyes were previously diagnosed with GA and collected consecutively from clinical practice. The study protocol was approved by an institutional review board, and the HIPAA compliant research adhered to the Declaration of Helsinki and all federal and state laws. Each 3D OCT data set was acquired over a 6×6 mm area (corresponding to 512×128 pixels) with a 1024-pixel (2 mm) axial resolution on a commercial SD-OCT device (Cirrus OCT; Carl Zeiss Meditec, Inc.).

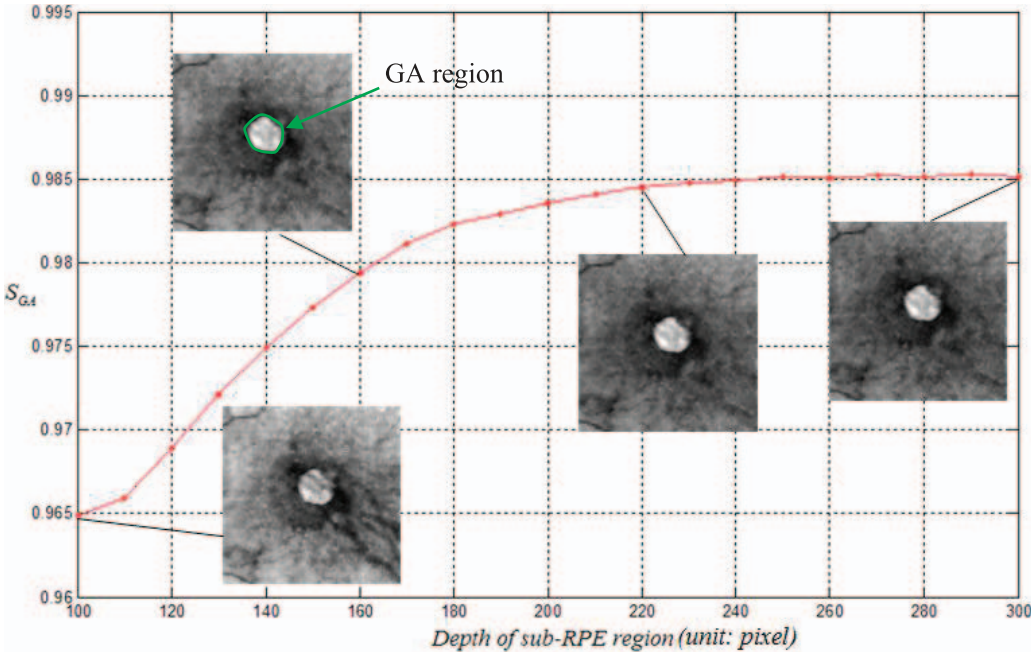

Figure 6. Depth of sub-RPE region for GA separability for one SD-OCT scan. Four GA projection images corresponding to *four red points* are inset.

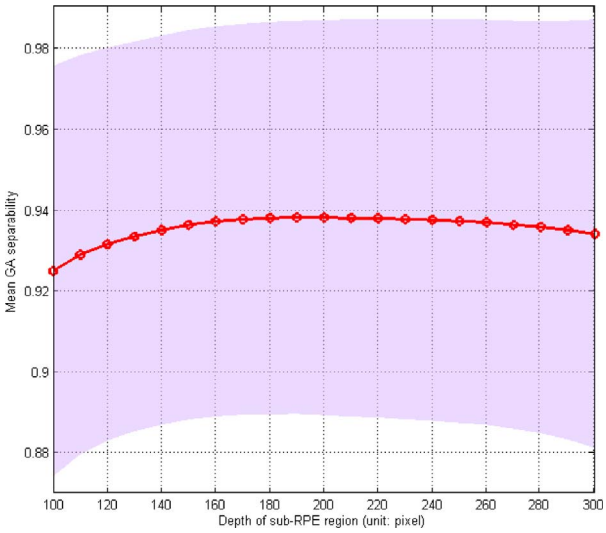

Figure 7. Mean (*redline*) and standard deviation (*pale pink shading*) of the GA separability across the 99 SD-OCT images in this study, considering different values of depth of sub-RPE region.

Both qualitative analysis and quantitative evaluations were performed on the data. For the quantitative evaluation, we computed two metrics to measure the GA contrast and distinction:

Mean difference (MD) between GA and background regions, defined by:

$$MD = \frac{\mu_{GA} - \mu_{bg}}{\mu_{GA} + \mu_{bg}} \quad (1)$$

where μ_{GA} and μ_{bg} represent the average intensity values in GA and background regions, respectively. The GA and background regions are outlined manually in GA projection images. An example manual annotation of the GA boundaries is shown in the top-left image in Figure 6 marked with a green outline. We used the MD to measure GA contrast against background regions. Higher MD values corresponded to higher contrast levels.

GA separability of the GA projection image was defined as:

$$S_{GA} = 1 - \frac{\max^{254}_{i=1} \sum_{j=1}^{K} |B_i(j) - G(j)|}{K} \quad (2)$$

where B_i indicates the binarized result with a global threshold of value i, with the GA projection image normalized to the interval [0, 255], and G indicates a GA segmentation result outlined manually. K denotes the number of the pixel in the GA projection image. In B_i and G, the GA and background regions are binarized to 1 and 0, respectively. The reasoning behind Equation 2 is to calculate the maximum overlap ratio between all of the binarization results generated with the global threshold and a "gold standard" outlined in the SVP projection images by an expert ophthalmic grader. The range of separability values is from 0 to 1. The best GA separability (i.e., $S_{GA} = 1$) represents the GA regions that can be completely separated from the background by a global threshold, namely the binarization results generated with the global threshold and the "gold standard" are the same. This metric was used to measure the GA distinction. Since one purpose of generating GA projection images is to reliably determine GA extent,[28] this separability measurement reflects the feasibility in the generated images.

Results

The proposed RSAP technique was tested and compared with the SVP and Sub-RPE Slab techniques qualitatively and quantitatively. The influence of the parameter controlling the maximum considered depth for the sub-RPE region, mentioned earlier, was first evaluated and later fixed for all 99 test images.

Parameter Evaluation

Figure 6 shows the GA separability for different depths of sub-RPE regions in one SD-OCT image, where the depth was varied from 100 to 300 pixels (approximately 0.2∼0.6 mm in the collected images) with an interval of 10 pixels. Figure 6 demonstrates that the GA separability increases when the depth increases from 100 to 240 pixels, and then remains stable with further depth increases. Figure 7 shows the relationship

Table 1. Average MD and SGA of the SVP, Sub-RPE Slab and RSAP Projection Images

Methods Compared	Number of Eyes/Cubes	MD	SGA
SVP	27/99	0.129	0.88
Sub-RPE Slab	27/99	0.238	0.919
RSAP	27/99	0.276	0.938

between the mean and standard deviation of the GA separability and the depth of sub-RPE region for all 99 SD-OCT images, which indicates an optimal depth range from 190 to 210 pixels (approximately 0.37∼0.41 mm). When the depth of sub-RPE region is much smaller than the axial region where GA can be observed in the SD-OCT images, the GA separability is low because only a limited region of the high-intensity values associated with GA near the BM are used. When this depth is increased to values that are larger than optimal, the GA separability decreases because more background intensity in sclera is included. In this paper, the depth of sub-RPE region was set to be 200 pixels (∼0.39 mm) for all test images.

Quantitative Results and Qualitative Analysis

Table 1 shows the average performance of the three tested techniques, where all of 99 cubes (3D SD-OCT images) from 27 eyes in 21 patients are used. Figure 8 shows the MD and separability values for each case included in our analysis.

Figures 9A to C show the GA projection images generated from the SD-OCT scan of a patient's left eye using the three techniques tested, SVP, Sub-RPE Slab, and RSAP, respectively. Figure 9D shows a one-line profile of the rows of Figures 9A to C marked with a dashed yellow line. The region marked with the dashed black oval in Figure 9D corresponds to the bright regions in the GA projection images (Figs. 9A–C).

Another example comparison of the SVP, Sub-RPE Slab and RSAP projection images is shown in Figures 10A to 10C, respectively. Figure 10D shows the results in the region of interest marked with the red dashed rectangle in Figure 10A, and Figure 10E shows one B-scan corresponding to the row in the GA projection images marked with a dashed yellow line.

Discussion

We have presented a novel technique, the RSAP, to increase the contrast and distinction of GA in a fundus projection image. In addition, we compared the images produced with the ones produced by two known methods, the SVP and Sub-RPE Slab techniques. Identifying and quantifying GA area is becoming more important in the diagnosis and management of advanced dry AMD.[11] With the development of pharmacologic and cell-based therapies for GA, accurately identifying and monitoring GA over time will be important in order to clinically determine the efficacy or failures of these novel treatment modalities.[29,30] Although SD-OCT has the potential to become the preferable technique for imaging the retina, direct visualization of GA in SD-OCT has been limited by low contrast and overlapping of retinal pathologies and structures when

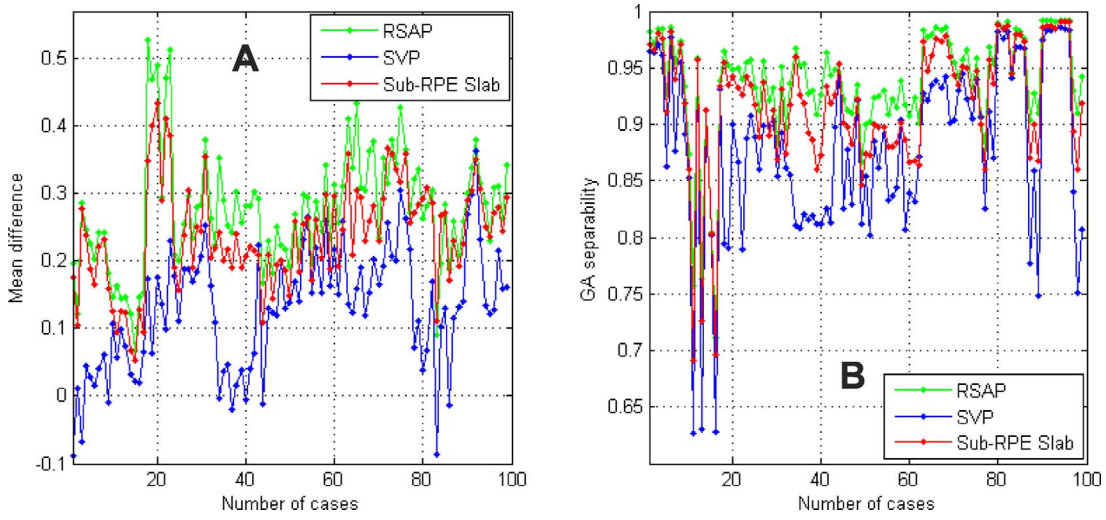

Figure 8. Comparison of the three tested GA projection techniques. (A) Mean difference. (B) GA separability.

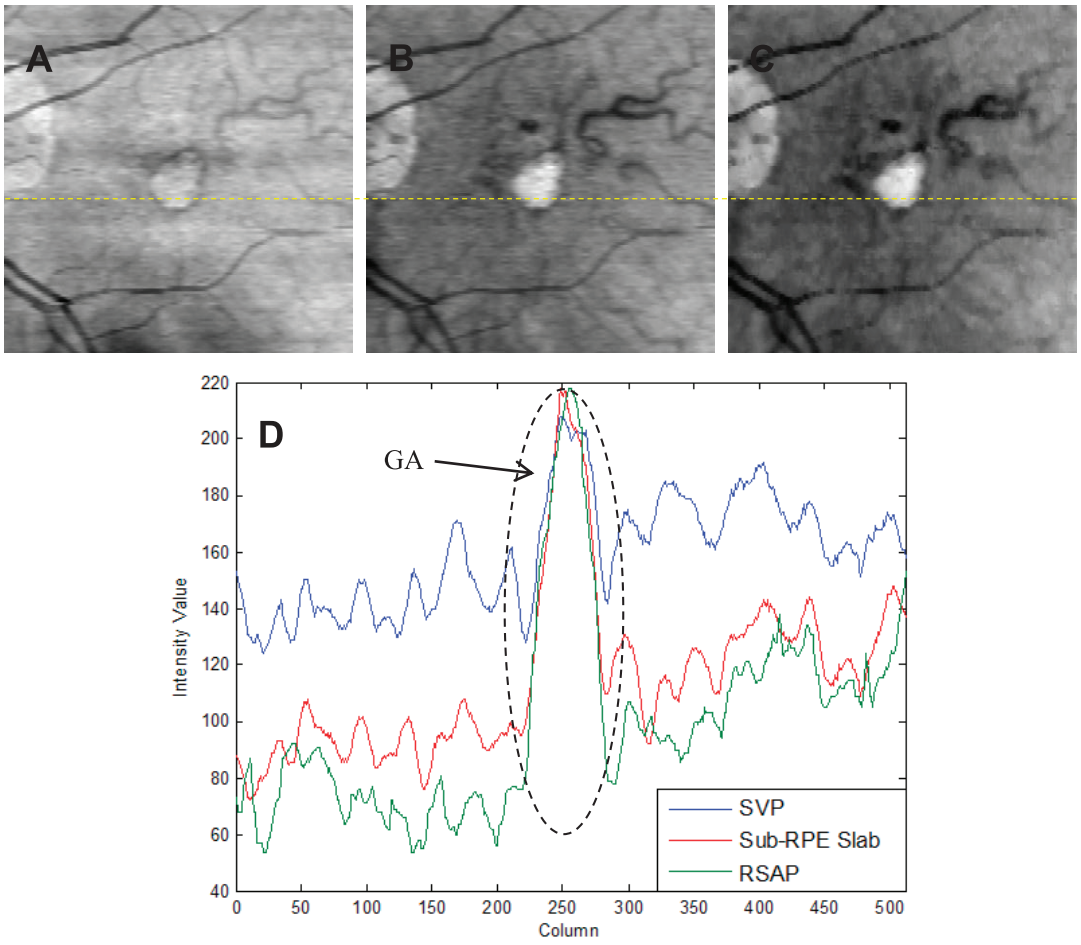

Figure 9. Comparison of three GA projection techniques in the left eye of one patient. (A) SVP. (B) Sub-RPE Slab. (C) RSAP. (D) One-line profile.

generating a fundus image. The RSAP method presented here improves direct visualization of GA by considering a restricted projection and the contribution of the choroidal vasculature.

We did not adopt the overlap ratio of the number of visualized lesions proposed in other studies [16,22] to evaluate performance across techniques, as GA presence can be easily identified with each technique, but rather we focused on the contrast and distinction between the GA and background regions among different techniques. Based on these proposed two metrics, the SVP technique had the lowest performance in the cases evaluated, while our technique (RSAP) had the highest performance (Table 1).

GA separability with the RSAP technique was higher than both the SVP and Sub-RPE Slab techniques and the RSAP technique produced images with a higher MD between GA and background regions for most of cases (Fig. 8). For several cases, the MD values of SVP are lower than 0 (Fig. 8A), implying that in these SVP projection images the average intensity values in GA regions are lower than that in background regions. For most cases (90/99 = 91%) the GA separability of the RSAP projection images is higher than 0.9 (Fig. 8B), suggesting a relatively high GA segmentation precision in RSAP projection images if an optimum global threshold can be obtained.

Figure 9 displays an example where the GA contrast in the SVP projection image (Fig. 9A) is too low to be able to easily distinguish the GA regions. The Sub-RPE Slab (Fig. 9B) and RSAP (Fig. 9C) projection images have a relatively good contrast for GA visualization. The RSAP projection image has the best contrast because the background intensity near the GA boundary is the lowest (the green line is below the blue and red lines as shown in Fig. 9D). The intensity gradient of the GA boundary is higher in the RSAP projection image than that in the SVP and Sub-

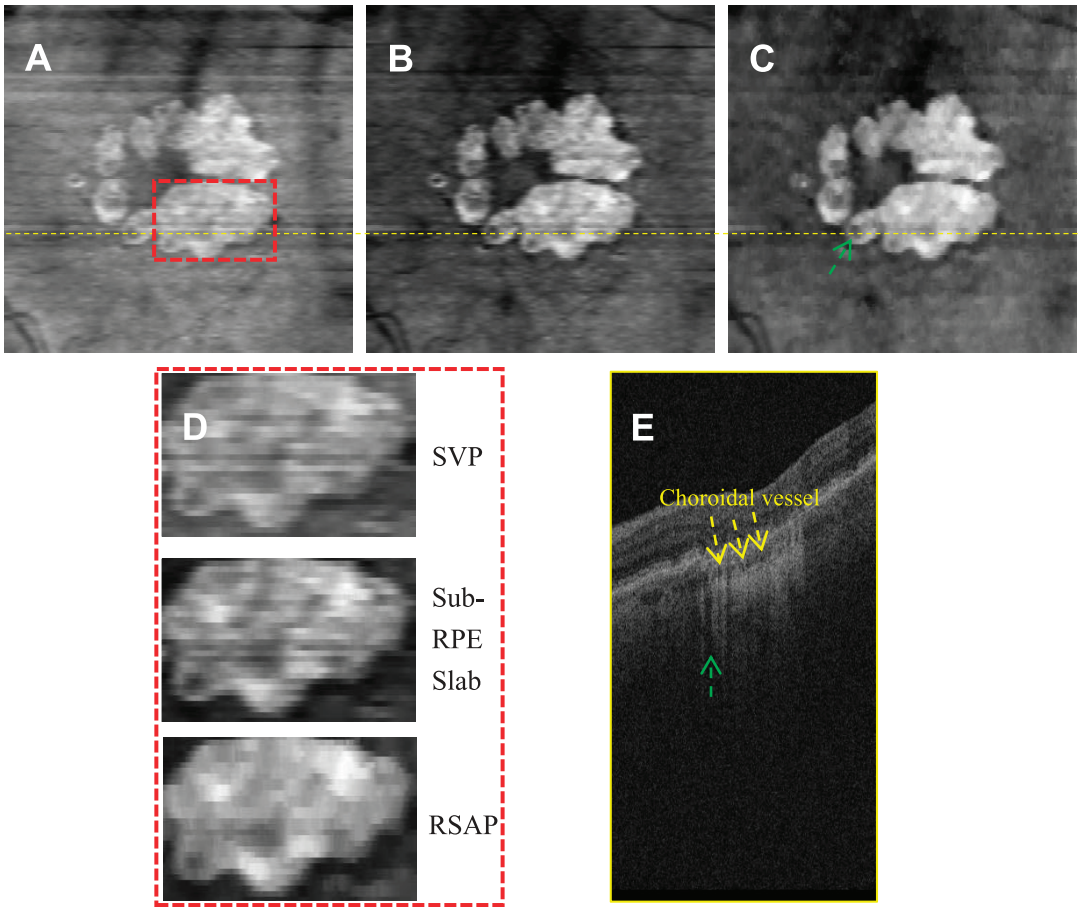

Figure 10. Qualitative comparison of GA visualization in a patient's left eye. (A) SVP. (B) Sub-RPE Slab. (C) RSAP. (D) Detail in region of interest for the three tested techniques. (E) Example B-scan at the location marked by the *dashed yellow line* in (A–C).

RPE Slab projection images, which would be helpful for enabling automated GA segmentation algorithms.

From Figure 10, we can observe that the GA contrast of the Sub-RPE Slab and RSAP projection images is better than that of the SVP projection image because these two region-restricted techniques exclude highly reflective retinal layers above the BM The intensity throughout the GA regions in the RSAP projection image also seems more consistent than in both the SVP and Sub-RPE Slab projection images because the choroidal vessel influence (marked with three dashed yellow arrows in Fig. 10E) has been excluded in our technique. However, the RSAP technique still presents some limitations: due to the lower intensity stripes in the choroidal and scleral regions (marked with the dashed green arrow in Fig. 10E), there are still dark areas within GA regions, as marked with the dashed green arrow in Figure 10C. On the other hand, this limitation also exists in the SVP and Sub-RPE Slab projection images. It appears that the dark stripes correspond to the presence of retinal vessels, suggesting that one solution may be to detect and exclude the retinal vessels before generating GA projection images in a similar manner as that which is done for the choroid vessels in this work. This will be a matter for future work.

In conclusion, we present a projection technique from 3D SD-OCT images based on intensity distribution in sub-RPE regions for the visualization of GA, which we called the RSAP technique. The RSAP technique improves on the previous methods by considering and using the intensity distribution characteristics in sub-RPE regions. Quantitative comparison in 99 3D SD-OCT scans from 21 patients demonstrated that the RSAP is more effective for GA visualization than the SVP and Sub-RPE Slab due to increased GA contrast and distinction.

Acknowledgments

Supported by a grant from the Fundamental Research Funds for the Central Universities (30920140111004), a six talent peaks project in Jiangsu Province (2014-SWYY-024), the Qing Lan Project, the Bio-X Interdisciplinary Initiatives Program of Stanford University, and a Spectrum-SPADA innovation grant from Stanford University (NIH-NCATS-CTSA-SPECTRUM).

References

1. Bird AC, Bressler NM, Bressler SB, et al. An international classification and grading system for age-related maculopathy and age-related macular degeneration. The International ARM Epidemiology Study Group. *Surv Ophthalmol*. 1995;39:367–374.
2. Resnikoff S, Pascolini D, Etya'als D, et al. Global data on visual impairment in the year 2002. *Bull World Health Organ*. 2004;82:844–851.
3. Bressler NM, Bressler SB, Fine SL. Age-related macular degeneration. *Surv Ophthalmol*. 1988;32:375–413.
4. Sunness JS, Gonzalez-Baron J, Applegate CA, et al. Enlargement of atrophy and visual acuity loss in the geographic atrophy form of age-related macular degeneration. *Ophthalmology*. 1999;106:1768–1779.
5. Yehoshua Z, Rosenfeld PJ, Albini TA. Current clinical trials in dry AMD and the definition of appropriate clinical outcome measures. *Semin Ophthalmol*. 2011;26:167–180.
6. Bearelly S, Chau FY, Koreishi A, et al. Spectral domain optical coherence tomography imaging of geographic atrophy margins. *Ophthalmol*. 2009;116:1762–1769.
7. Dunaief JL, Dentchev T, Ying GS, Milam AH. The role of apoptosis in age-related macular degeneration. *Arch Ophthalmol*. 2002;120:1435–1442.
8. Lutty G, Grunwald J, Majji AB, Uyama M, Yoneya S. Changes in choriocapillaris and retinal pigment epithelium in age-related macular degeneration. *Mol Vis*. 1999;5:35.
9. McLeod DS, Taomoto M, Otsuji T, et al. Quantifying changes in RPE and choroidal vasculature in eyes with age-related macular degeneration. *Invest Ophthalmol Vis Sci*. 2002;43:1986–1993.
10. Gregori G, Wang F, Rosenfeld PJ, et al. Spectral domain optical coherence tomography imaging of drusen in nonexudative age-related macular degeneration. *Ophthalmol*. 2011;118:1373–1379.
11. Yehoshua Z, Rosenfeld PJ, Grgori G, et al. Progression of geographic atrophy in age related macular degeneration imaged with spectral domain optical coherence tomography. *Ophthalmology*. 2011;118:679–686.
12. Fleckenstein M, Schmitz-Valckenberg S, Martens C, et al. Fundus autofluorescence and spectral-domain optical coherence tomography characteristics in a rapidly progressing form of geographic atrophy. *Invest Ophthalmol Vis Sci*. 2011;52:3761–3766.
13. Fleckenstein M, Schmitz-Valckenberg S, Adrion C, et al. Tracking progression with spectral-domain optical coherence tomography in geographic atrophy caused by age-related macular degeneration. *Invest Ophthalmol Vis Sci*. 2010;51:3846–3852.
14. Gobel AP, Fleckenstein M, Schmitz-Valckenberg S, Brinkmann CK, Holz FG. Imaging geographic atrophy in age-related macular degeneration. *Ophthalmologica,* 2011;226;182–190.
15. Bindewald A, Bird AC, Dandekar SS, et al. Classification of fundus autofluorescence patterns in early age-related macular disease. *Invest Ophthalmol Vis Sci*. 2005;46:3309–3314.
16. Schmitz-Valckenberg S, Fleckenstein M, Gobel AP, Hohman TC, Holz FG. Optical coherence tomography and autofluorescence findings in areas with geographic atrophy due to age-related macular degeneration. *Invest Ophthalmol Vis Sci*. 2011;52:1–6.
17. Sayegh RG, Simader C, Scheschy U, et al. A systematic comparison of spectral-domain optical coherence tomography and fundus autofluorescence in patients with geographic atrophy. *Ophthalmology*. 2011;118:1844–1851.
18. Chen Q, Leng T, Zheng LL, Kutzscher L, De Sisternes L, Rubin DL. An improved optical coherence tomography-derived fundus projection image for drusen visualization. *Retina,* 2014;34:996–1005.
19. Jiao S, Knighton R, Huang X, Gregori G, Puliafito C. Simultaneous acquisition of sectional and fundus ophthalmic images with spectral-domain optical coherence tomography. *Opt Express*. 2005;13:444–452.

20. Khanifar AA, Koreishi AF, Izatt Ja, Toth CA. Drusen ultrastructure imaging with spectral domain optical coherence tomography in age-related macular degeneration. *Ophthalmol*. 2008; 115:1883–1890.
21. Wojtkowski M, Srinivasan V, Fujimoto JG, et al. Three-dimensional retinal imaging with high-speed ultrahigh-resolution optical coherence tomography. *Ophthalmol*. 2005;112:1734–1746.
22. Stopa M, Bower BA, Davies E, et al. Correlation of pathologica features in spectral domain optical coherence tomography with conventional retinal studies. *Retina*. 2008;28:298–308.
23. Yehoshua Z, Garcia Filho CA, Penha FM, et al. Comparison of geographic atrophy measurements from the OCT fundus image and the sub-RPE slab image. *Ophthalmic Surg Lasers Imaging Retina*. 2013;44:127–132.
24. Chen Q, Leng T, Niu S, et al. A false color fusion strategy for drusen and GA visualization in OCT images. *Retina*. 2014;34:2346–2358.
25. Stetson PF, Yehoshua Z, Garcia Filho CA, et al. OCT minimum intensity as a predictor of geographic atrophy enlargement. *Invest Ophthalmol Vis Sci*. 2014;55:792–800.
26. Hogan MJ, Alvarado JA, Wddell JE. Histology of the human eye. Philadelphia: W.B. Saunders Co.; 1971.
27. Garvin MK, Abràmoff MD, Wu X, Russell SR, Burns TL, Sonka M. Automated 3-D intraretinal layer segmentation of macular spectral-domain optical coherence tomography images. *IEEE Trans Med Imaging*. 2009;28:1436–1447.
28. Chen Q, De Sisternes L, Leng T, Zheng LL, Kutzscher L, Rubin DL. Semi-automatic geographic atrophy segmentation for SD-OCT images. *Biomed Optics Exp*. 2013;4:2729–2750.
29. Volz C, Pauly D. Antibody therapies and their challenges in the treatment of age-related macular degeneration. *Eur J Pharm Biopharm*. 2015;pii: S0939-6411(15)00102-2.
30. Zhang K, Hopkins JJ, Heier JS, et al. Ciliary neurotrophic factor delivered by encapsulated cell intraocular implants for treatment of geographic atrophy in age-related macular degeneration. *Proc Natl Acad Sci U S A*. 2011;108:6241–6245.